Int. J. Electrochem. Sci., 15 **(2020)** 11757 – 11768, doi: 10.20964/2020.12.70

International Journal of
ELECTROCHEMICAL
SCIENCE
www.electrochemsci.org

Electrochemical Investigation of Polypyrrole/Nd_2O_3 Nanocomposite as High Performance Supercapacitor Material on Mild Steel Substrate

F. Abdollahi, M. Shahidi-Zandi[*], *M.M. Foroughi, M. Kazemipour*

Department of Chemistry, Kerman Branch, Islamic Azad University, Kerman, Iran.
[*]E-mail: meshahidizandi@gmail.com

Received: 5 July 2019 / *Accepted:* 24 October 2019 / *Published:* 31 October 2020

The PPy films prepared on the mild steel substrate in the absence of the non-conductive iron(II) oxalate layer can be used as the effective electrodes for electrochemical supercapacitors. This study introduces a nanocomposite material for electrochemical redox capacitors, which has advantages, such as long life cycle and stability in an aqueous electrolyte. A polypyrrole/Nd_2O_3 thin film electrode was synthesized electrochemically as an electrochemical supercapacitor. The supercapacitive performance of the PPy/Nd_2O_3 coated electrode was investigated in 0.1 M H_2SO_4 solution using cyclic voltammetry (CV), galvanostatic charge–discharge and electrochemical impedance spectroscopy (EIS) techniques. The calculated specific capacitance of the PPy and PPy/Nd_2O_3 electrodes using the CV method was 119 and 259 $F.g^{-1}$, respectively. The PPy/Nd_2O_3 nanocomposite as a capacitor material has shown some advantages such as long life cycle and stability in an aqueous electrolyte. The retention of capacitance after 3000 cycles was about 88% of the initial capacitance at the current density of 1 $A.g^{-1}$. According to EIS data, the supercapacitor using PPy/Nd_2O_3 nanocomposite material on mild steel substrate has high specific capacitance of 268 $F.g^{-1}$ compared with 125 $F.g^{-1}$ for PPy coating.

Keywords: Electrosynthesized polypyrrole; Supercapacitor; Nd_2O_3 Nanorods; Electrochemical impedance spectroscopy.

1. INTRODUCTION

The need to develop the clean energy systems has increased the research on energy storage devices [1]. The supercapacitors can store and deliver a larger amount of power comparing to the batteries [2, 3]. The supercapacitors can be classified into two categories: (1) electrical double layer capacitors and (2) pseudocapacitors.

In the electrical double-layer types of supercapacitors the electrostatic charges of electrolyte accumulate on the surface of electrode without any redox reaction. The typical double-layer electrodes are carbon-based materials [4, 5]

In the pseudocapacitive types of supercapacitors the electrical energy is stored by electroactive materials through the rapid and reversible faradaic reactions on the surface of electrodes. Three types of faradaic reactions can occur on the electrodes: reversible surface adsorption of protons or metal ions from the electrolytes, redox reactions of transition metal oxides and reversible electrochemical doping/dedoping in conducting polymers.

According to the previous researches, the energy density of the pseudocapacitive materials including conducting polymers and transition metal oxides are relatively better than that of the double-layer capacitors [6, 7].

Conductive polymers and metal oxides are extensively used as electrode materials in the pseudocapacitive supercapacitor studies [3, 6, 8, 9]. Some of the studied metal oxides are ruthenium oxide [10], manganese oxide [11, 12], nickel oxide [13], cobalt oxide [14], zinc oxide [15] and vanadium oxide [16].

Conducting polymers are suitable for using in the fields such as supercapacitors, sensors, anti-corrosion coatings, and batteries [7, 9, 12, 17-20]. Polypyrrole (PPy) due to its advantages such as relatively easy polymerization, thermal stability and low cost is one of the most used conducting polymers [21-23].

The composite materials made of PPy and metal oxides are preferred over the use of only one of these two species in the supercapacitor researches due to the rapid degradation of PPy and the low conductivity of metal oxides. Thus, PPy acts as conducting support to the poor conducting nanosized metal oxide and further increased the performance.

The goal of this work was the electrodeposition of PPy coatings directly on mild steel substrate and investigation of electrochemical performance of the PPy films. To improve the capacitance performance of the PPy coated electrods, PPy/Nd_2O_3 nanocomposite was employed. The Nd_2O_3 nanorods were synthesized by pulse electrochemical deposition method. Then, PPy/Nd_2O_3 nanocomposite was synthesized by cyclic voltammetry in a solution containing pyrrole and Nd_2O_3 nanorods. The cyclic voltammetry, chrono-amperometry and charge-discharge measurements were employed to investigate the electrochemical properties of the PPy/Nd_2O_3 nanocomposite. The specific capacitance was calculated from both the CV and the galvanostatic charge-discharge cycling experiments.

2. EXPERIMENTAL

2.1 Materials

All chemicals materials were purchased from Merck. Pyrrole was distilled under vacuum for the purification purpose, and then it was stored in the dark below 5 ◦C. Solutions were prepared by using distilled water.

2.2 Methods

2.2.1 Preparation of Nd_2O_3 nanorods

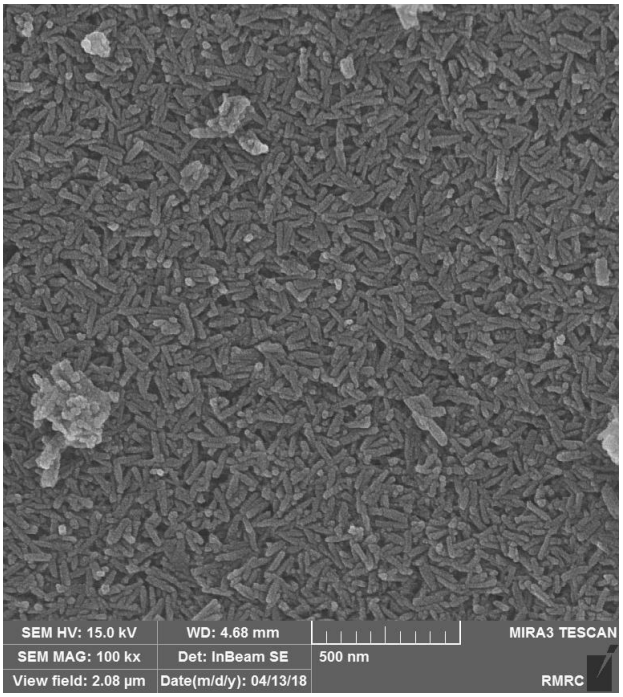

Figure 1. FESEM image of the prepared Nd_2O_3 nanorods

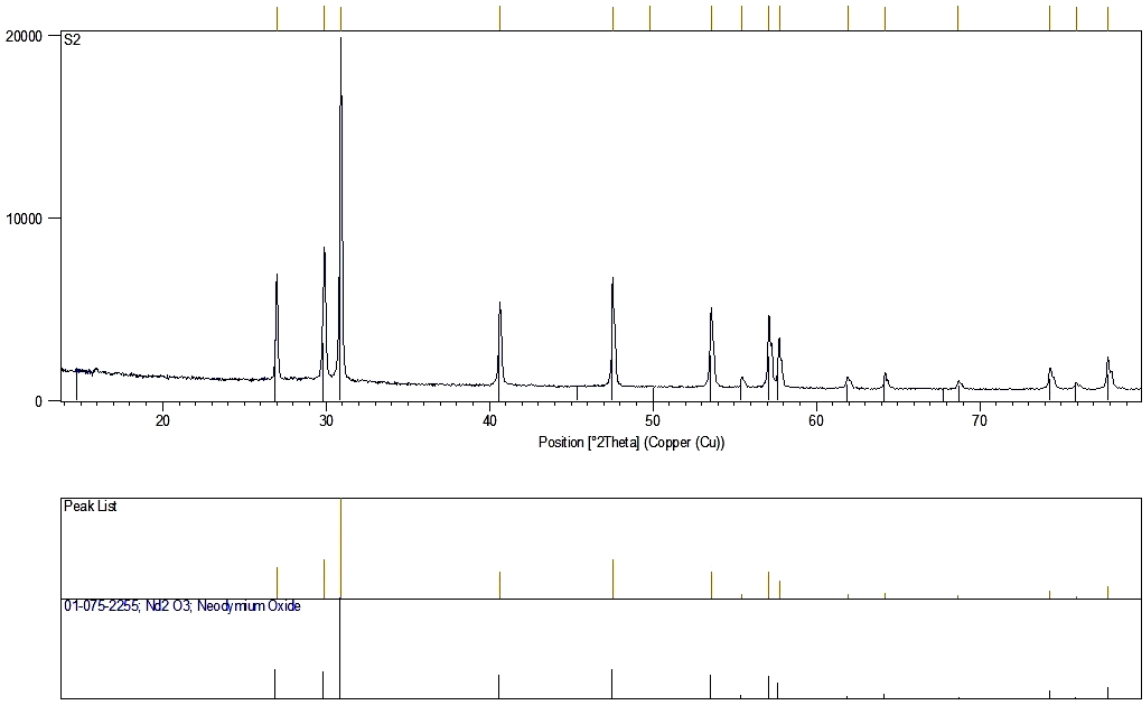

Figure 2. X-ray diffraction patterns of the prepared Nd_2O_3 nanorods

The cathodic pulse electrochemical deposition method was employed to synthesis Nd_2O_3 nanorods in a conventional three-electrode cell. The reference electrode was a saturated calomel electrode (SCE) and a 316 stainless steel plate (100×50×0.5 mm) was a working electrode centred between two parallel graphite plates (100×50×5 mm) as the counter electrodes.

The electrodes were immersed in the electrolyte solution containing 0.005 M $Nd(NO_3)_3.6H_2O$. The square wave potential (-2.1 V vs. SCE) was applied in the cathodic electrodeposition. The experiment was performed at the current density of 5 mA/cm^2 and $t_{on} = t_{off} = 1ms$ for 10 min at 353 K and pH=4.2. After the electrochemical deposition process, the stainless steel electrode was washed by distilled water followed by drying in air for 24 h. The scraped gels were treated at 1000 ^oC for 5 h by an electrical furnace with the heating rate of 10 ^oC/min. Figure 1 presents the FESEM image of Nd_2O_3 nanorods . Figure 2 shows the XRD pattern of Nd_2O_3 nanorods.

2.2.2 Preparation of PPy and PPy/Nd_2O_3 nanocomposite coated electrodes

A disk of mild steel (100 mm2), a saturated (KCl) Ag/AgCl and a platinum rod were used as working, reference and counter electrodes, respectively. After polishing the working electrode by wet abrasive papers (600-2500 grades) and washing with ethanol, the electropolymerization test was performed on the surface of the mild steel electrode immersed in 0.1 M KCl, 0.3 M oxalic acid and 0.1 M pyrrole solution containing 0.5% Nd_2O_3 nanorods by cyclic voltammetry technique. The same solution without Nd_2O_3 nanorods was employed for preparation of the PPy coated mild steel electrode. Ten consecutive cycles were used for the electropolymerization process at the scan rate of 50 mV.s^{-1} in potentials between 0.0 and 1 V (vs. Ag/AgCl).

The mass of PPy films was approximated using Faraday's law of electrolysis assuming 100% current efficiency for the electropolymerization process [24]:

$$m = \frac{Q(M_m + yM_a)}{(2+y)F} \quad (1)$$

where Q is the electrical charge for electrodeposition of PPy, M_m is the molecular weight of the monomer (67 g/mol), M_a is the molecular weight of the inserted anion (88 g/mol), y is the doping yield of the anions into PPy coating (generally y = 0.3), and F is the Faraday's constant.

2.2.3 EIS tests

A sinusoidal potential signal of 10 mV amplitude was employed in the frequency range of 100 kHz-10 mHz for electrochemical impedance spectroscopy (EIS) measurements. The EIS data were recorded by a potentiostat/galvanostat (Autolab Model PGSTAT-302N). A conventional three-electrode cell containing a saturated Ag/AgCl electrode as the reference electrode a Pt rod as the counter electrode, and the PPy coated mild steel as the working electrode was used to measure the EIS data. The experimental EIS plots were fitted to the equivalent circuit by the software of Nova 1.9.

3. RESULTS AND DISCUSSION

The main challenge of the electrodeposition of PPy coatings on the metallic substrates such as mild steel is the dissolution of the substrate at the potential required to oxidize the pyrrole monomer [23]. The addition of oxalic acid to the electrolyte solution is an effective way to overcome this problem [25]. The interaction of oxalic acid with the steel leads to form the passive layer of iron(II) oxalate on the steel surface which can prevent the dissolution of the steel substrate during the PPy electropolymerization process. However, the formation of the non-conductive and noncapacitive layer of iron(II) oxalate results in both increasing charge transfer resistance and reducing electrochemical capacitance of the PPy coated electrodes [26]. Some researchers employed an approach based on the use of an anionic additive with chelating properties, which facilitated the charge transfer and increased the electrochemical capacitance of the PPy electrodes [26, 27].

According to the mechanism presented by Su and Iroh, at the electropolymerization potential of pyrrole the formed passive layer of iron(II) oxalate on the steel substrate is oxidized to highly soluble iron(III) oxalate and thereby the PPy film is prepared on the steel substrate in the absence of the non-conductive iron(II) oxalate layer [25]. The PPy films deposited directly on the steel substrates can be used as the effective electrodes for electrochemical supercapacitors.

The electrochemical performance of PPy/Nd_2O_3 coated mild steel electrode was investigated by cyclic voltammetry technique. Figure 3 shows the CV curves of PPy and PPy/Nd_2O_3 coated mild steel electrodes immersed in 0.1M H_2SO_4 solution at the scan rate of 25 mV/s and the potential range of -0.1 – 0.8 V (vs. Ag-AgCl). It is clear that the capacitance of the PPy coating increased by doping the PPy matrix with Nd_2O_3 nonorods.

The structure and morphology of the coating material is an important factor that can influence in the capacity of electrochemical energy storage. Electrochemical supercapacitor performances of PPy/Nd_2O_3 electrodes were recorded in 0.1 M H_2SO_4 solution.

The following equation was employed to obtain the specific capacitance (C_S) of the electrodes from the CV curves [28]:

$$C_S = \frac{1}{m\nu(V_c - V_a)}\int_{V_a}^{V_c} I(V)dV \qquad (2)$$

where C_S is the specific capacitance (F/g), □□is the scan rate (mV/s), V_c-V_a is the potential range (−0.1 to 0.8 V vs Ag/AgCl), I is the response current (mA), and m is the deposited weight of the PPy material on the electrode surface per unit area (g/cm^2). The the specific capacitance ($C_{S)}$ of the PPy and PPy/Nd_2O_3 electrodes were found to be 119 and 259 F g^{-1}, respectively.

Figure 4 shows the CV curves of the PPy/Nd_2O_3 electrode in 0.1 M H_2SO_4 solution at different scan rates. It is apparent from the CV curves that the PPy/Nd_2O_3 electrode has an excellent capacitive performance. According to Figure 4, the current response of the PPy/Nd_2O_3 composite film increased with increasing the scan rate. The ideal capacitive behavior of the PPy/Nd_2O_3 electrode is the reason of this phenomenon.

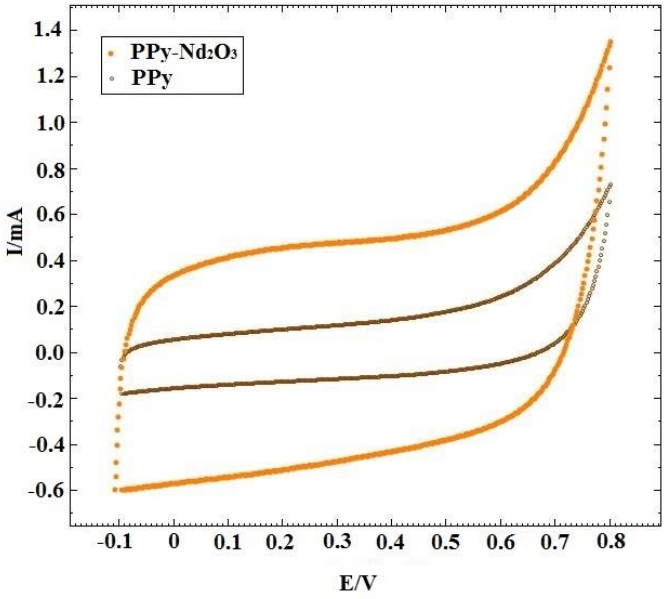

Figure 3. Cyclic voltammograms of the PPy and PPy/Nd_2O_3 coated mild steel electrodes in 0.1 M H_2SO_4 at the scan rate of 25 $mV.s^{-1}$ and the potential range of -0.1 – 0.8 V (vs. Ag-AgCl)

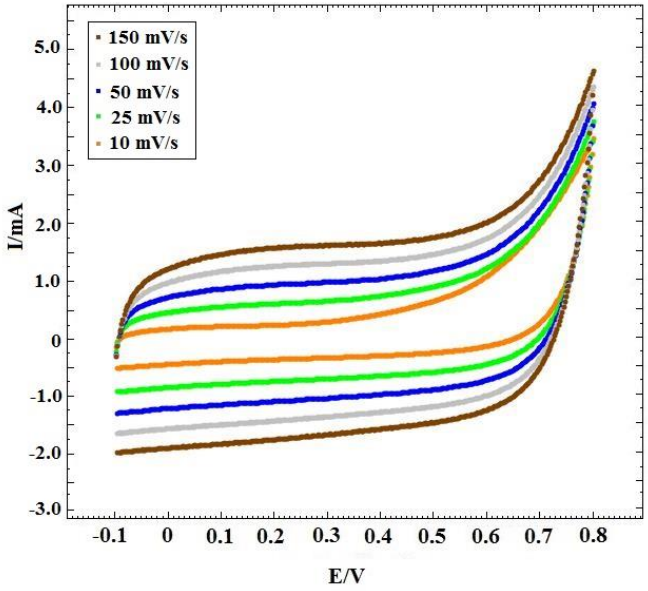

Figure 4. CVs of the PPy/Nd_2O_3 coated mild steel electrode in 0.1 M H_2SO_4 solution at different scan rates amd in the potential window of -0.1 – 0.8 V(vs. Ag-AgCl)

Figure 5 shows the plots of the calculated specific capacitance of the PPy and PPy/Nd_2O_3 electrodes versus the scan rate. It is clear that the capacitance of the two electrodes decays over the entire range of scan rate because of the accessibility of the outer pores rather than the inner pores for the doping/undoing process at the high scan rates. As Figure 5 shows, at the high scan rates the specific capacitance of the PPy/Nd_2O_3 electrode decreased with a decreasing pattern similar to the PPy electrode. Therefore, it can be concluded that the PPy/Nd_2O_3 have not blocked the pores of the polymer network.

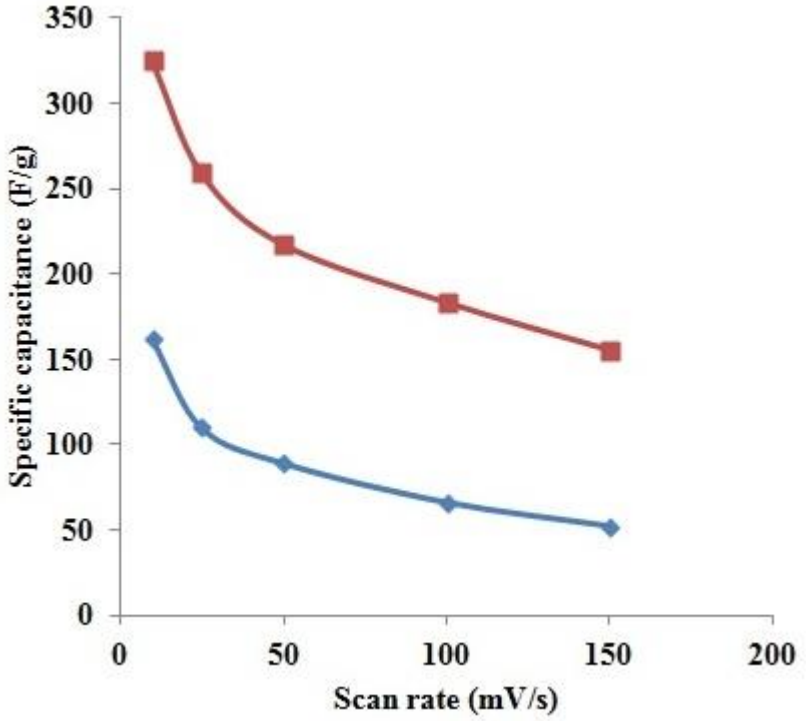

Figure 5. The plots of the calculated specific capacitances of the PPy and PPy/Nd_2O_3 coated mild steel electrodes at different scan rates in 0.1 M H_2SO_4 solution

The employment of the galvanostatic charge/discharge method was suitable to highlight the capacitance characteristic of the PPy/Nd_2O_3 coated mild steel electrode. The charge/discharge measurements of the PPy and PPy/Nd_2O_3 coated mild steel electrodes at the current density of 2.0 $A.g^{-1}$in the potential range of 0 to 0.8 V are shown in Figure 6. Both the good columbic efficiency and ideal capacitive behavior of PPy/Nd_2O_3 coated mild steel as an electrode for supercapacitor applications are apparent from a triangular shape between the potential ranges.

Figure 7 shows the charge–discharge plots of the PPy/Nd_2O_3 coated mild steel electrode at different specific currents of 2–15 $A.g^{-1}$. The capacitive behavior of the PPy/Nd_2O_3 coated mild steel electrode is apparent from the linear shape of the charge and discharge plots in agreement with the data of CV plots. According to Figure7, the specific capacitance values decreased with increasing the specific current due to the intercalation of ions at the surface of the coating materials. On the other hand, the specific capacitance increased with decreasing the specific current because there is the enough time for insertion and deinsertion of the ions at the outer and inner pores of the polymer coatings.

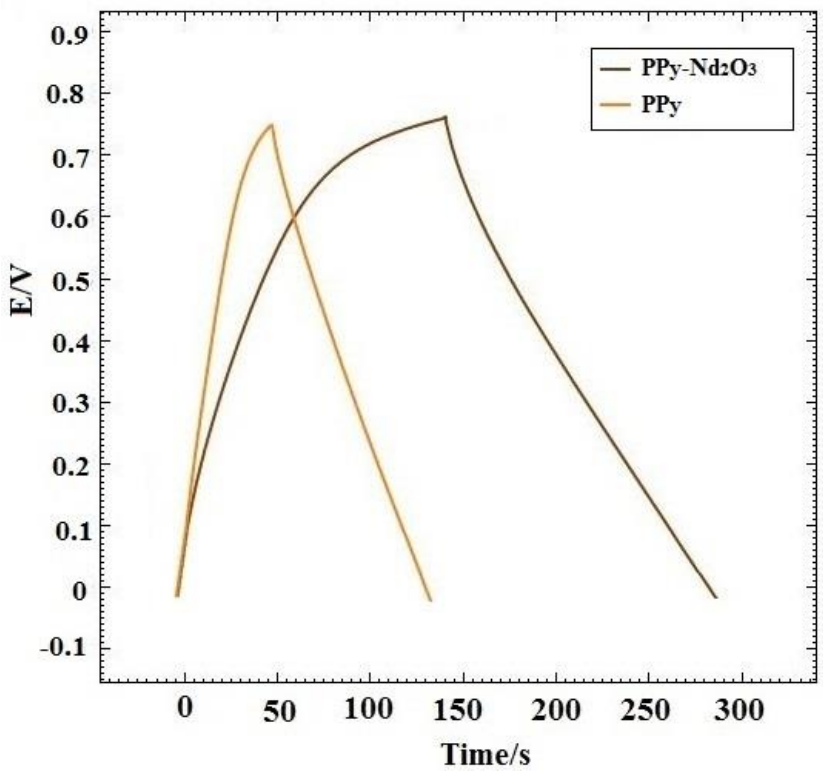

Figure 6. Charge-discharge measurements of the PPy and PPy/Nd_2O_3 coated mild steel electrodes in 0.1 M H_2SO_4 solution at the current density of 2.0 A g^{-1} and in the potential range of 0 to 0.8 V (vs. Ag-AgCl)

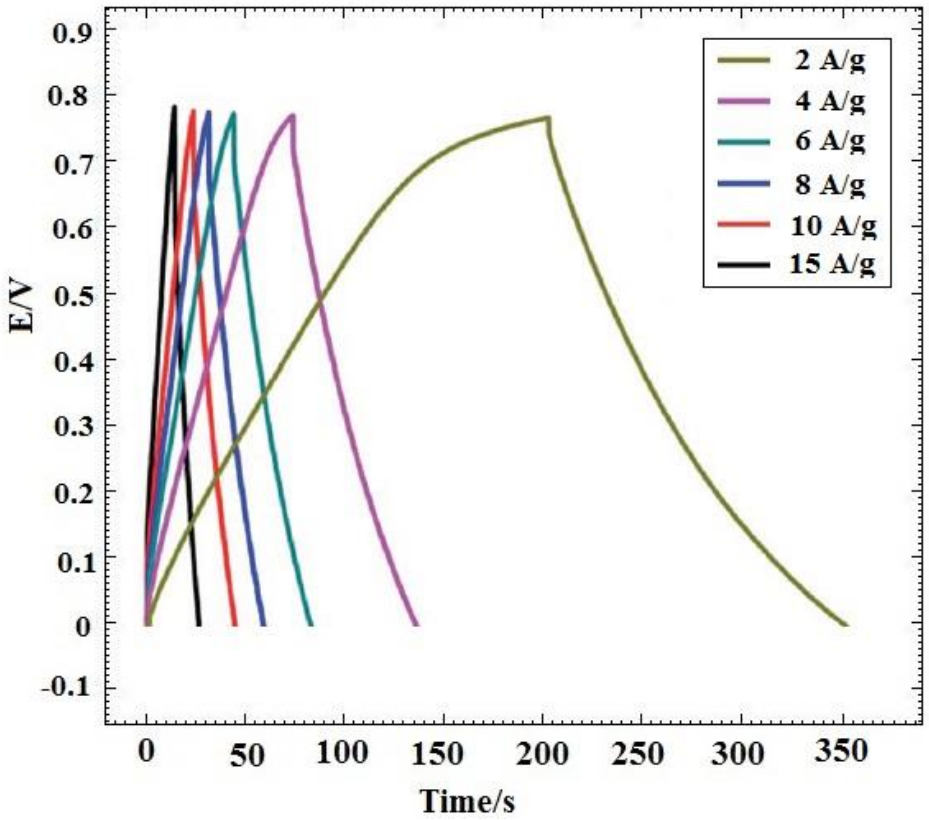

Figure 7. Charge-discharge curves of PPy/Nd_2O_3 coated mild steel electrode in 0.1 M H_2SO_4 solution at different current densities and in the potential range of 0 to 0.8 V (vs. Ag-AgCl)

The PPy/Nd_2O_3 coated mild steel electrode exhibits the specific capacitance of 185 F g^{-1} at high discharge current density (15 A g^{-1}). The high capacitance at high discharge current density is mainly due to the porous and thereby high surface area of the coating materials which provides more surface area for performing the redox reactions.

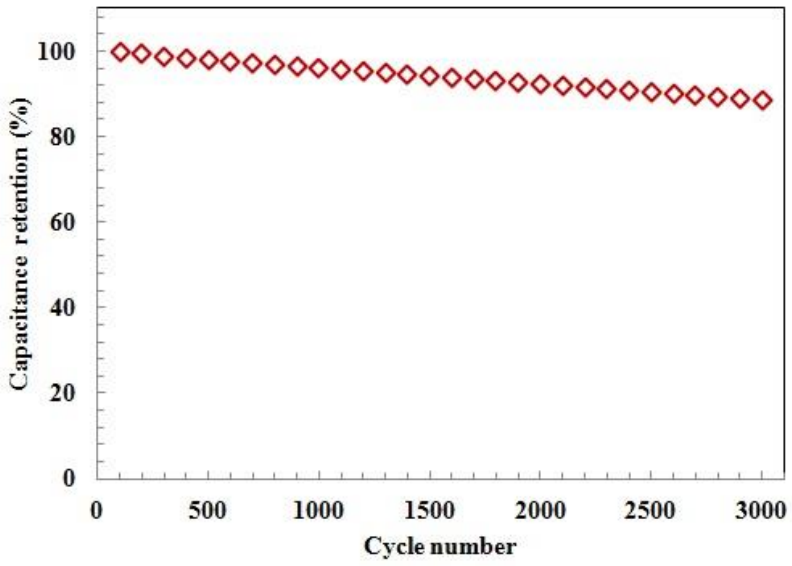

Figure 8. Percent capacitance retention vs cycle number (up to 3000 cycles of charge-discharge) at the specific current 1 A g^{-1} for as prepared of PPy/Nd_2O_3 coated mild steel electrode

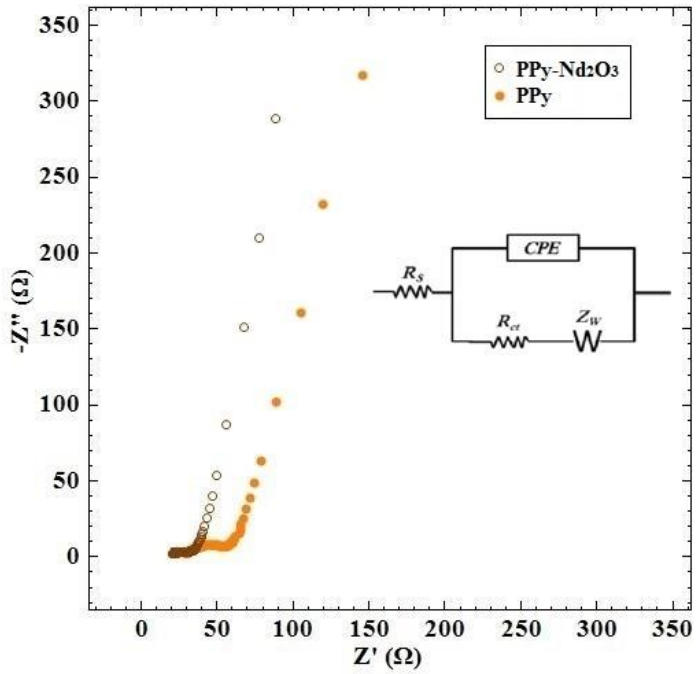

Figure 9. Nyquist plots for the PPy and PPy/Nd_2O_3 coated mild steel electrodes and the equivalent circuit

Figure 8 shows the galvanostatic charge-discharge cycling data of the electrode of PPy/Nd_2O_3 subjecting to the long charge-discharge cycling test at the current density of 1 $A.g^{-1}$. The specific capacitance slightly decreased from 259 $F.g^{-1}$ to 229 $F.g^{-1}$ after 3000 cycles of charge-discharge. Therefor, the capacity retention is about 88% after 3000 cycles of charge-discharge. According to these results, the PPy/Nd_2O_3 electrode presented high degree of cycling stability and the excellent reversibility on repetitive charge-discharge cycling. The capacity retention on the electrochemical cycling is due to the nature of porous PPy/Nd_2O_3 nano composite possessing high surface area.

The electrochemical behavior of the prepared PPy/Nd_2O_3 coated mild steel electrode was investigated by the EIS technique. The Nyquist plots of the PPy and PPy/Nd_2O_3 coated mild steel electrodes are shown in Figure 9. The semicircle at high frequencies is related to the charge transfer resistance (R_{ct}) arising from the faradic reactions and the double-layer capacitance (C_{dl}) at the interface between the electrode and electrolyte solution [29, 30]. The Warburg resistance (Z_W) is resulted from the frequency dependence of ion diffusion in the electrolyte solution. It is clear that the R_{ct} value of the PPy/Nd_2O_3 electrode was smaller than that of the PPy electrode. Therefore, the inserting of Nd_2O_3 nonorods into the PPy film improves the charge transfer performance of the PPy coating. Both the PPy and PPy/Nd_2O_3 electrodes exhibit an almost linear behavior in the low frequency region of the Nyquist plot. This indicates that the diffusion resistance of the electrolyte ions into the electrode was decreased, as expected for a capacitor. The low frequency capacitance (C_{lf}) of each film was determined from the following equation [31]:

$$C_{lf} = 1/\left(2\pi f Z''\right) \quad (3)$$

The specific capacitance for the PPy and PPy/Nd_2O_3 coated mild steel electrodes was determined to be 125 and 268 F g^{-1}, respectively. It is clear that the capacitance of the PPy/Nd_2O_3 electrode was higher than that of the PPy electrode. These results confirmed the results of the CV and charge–discharge measurements.

Table 1 lists the capacitance performance of different nanostructured electrodes in comparison with the present work. In addition, the analysis of literature showed that the highest specific capacitance of 343 $F.g^{-1}$ was observed at 2 $mV.s^{-1}$ for the PPy films prepared on stainless steel substrates [26]. The specific capacitance decreased with increasing scan rate.

Table 1. Different nanostructures electrodes and their capacitance performance.

Samples	Specific capacitance	Electrolyte	Capacitance retention	Ref
Aerogels	184 $F.g^{-1}$ at 0.5 $A.g^{-1}$	H_2SO_4	57%	[32]
Nanofibers	252 $F.g^{-1}$ at 0.5 $A.g^{-1}$	H_2SO_4	62%	[33]
Nanoporous	350 $F.g^{-1}$ at 1 $A.g^{-1}$	H_2SO_4	90%	[34]
Nanospheres	345 $F.g^{-1}$ at 1 $A.g^{-1}$	H_2SO_4	91%	[35]
Nanosheets	272 $F.g^{-1}$ at 1 $A.g^{-1}$	H_2SO_4	34%	[36]
Nanorods	297 $F.g^{-1}$ at 1 $A.g^{-1}$	H_2SO_4	-	[37]
Nanorods	268 $F.g^{-1}$ at 1 $A.g^{-1}$	H_2SO_4	88%	This work

4. CONCLUSION

A polypyrrole/Nd_2O_3 thin film synthesized directly on the mild steel substrate was used as an effective electrode for electrochemical supercapacitor. The applicability of the system as a supercapacitor was investigated by several electrochemical techniques, including cyclic voltammetry, galvanostatic charge–discharge experiments and electrochemical impedance spectroscopy. Based on the electrochemical results obtained, PPy/Nd_2O_3 gave higher specific capacitance. The supercapacitor using PPy/Nd_2O_3 nanocomposite material has high specific capacitance of 259 $F.g^{-1}$ compared with 119 $F.g^{-1}$ for the PPy coating. The PPy/Nd_2O_3 nanocomposite as a capacitor material has shown advantages such as long life cycle and stability in an aqueous electrolyte. The capacitance retention after 3000 cycles is about 88% of the initial capacitance at the current density of 1 $A.g^{-1}$.

References

1. W. Xie. X. Jiang. T. Qin. H. Yang. D. Liu, D. He. *Electrochim. Acta*, 258 (2017) 1064.
2. J. Zhang. S. Song. Y. Chen. S. Huang. P. Li, H. Luo. *Appl. Surf. Sci.*, 442 (2018) 750.
3. Z. S. Iro. C. Subramani, S. S. Dash. *Int. J. Electrochem. Sci.*, 11 (2016) 10628.
4. T. Leydecker. M. Eredia. F. Liscio. S. Milita. G. Melinte. O. Ersen. M. Sommer. A. Ciesielski, P. Samorì. *Carbon*, 130 (2018) 495.
5. E. Taer. A. Apriwandi. Y. S. Ningsih. R. Taslim, Agustino. *Int. J. Electrochem. Sci.*, 14 (2019) 2462.
6. P. Simon. Y. Gogotsi, B. Dunn. *Science*, 343 (2014) 1210.
7. E. Karaca. D. Gökcen. N. Ö. Pekmez, K. Pekmez. *Electrochim. Acta*, 305 (2019) 502.
8. L. Yuan. B. Yao. B. Hu. K. Huo. W. Chen, J. Zhou. *Energy Environ. Sci.*, 6 (2013) 470.
9. L. Huang. W. Rao. L. Fan. J. Xu. Z. Bai. W. Xu, H. Bao. *Polymers*, 10 (2018) 135.
10. J. Zang. S.-J. Bao. C. M. Li. H. Bian. X. Cui. Q. Bao. C. Q. Sun. J. Guo, K. Lian. *J. Phys. Chem. C*, 112 (2008) 14843.
11. G. Han. Y. Liu. L. Zhang. E. Kan. S. Zhang. J. Tang, W. Tang. *Sci. Rep.*, 4 (2014) 4824.
12. A. Bahloul. B. Nessark. E. Briot. H. Groult. A. Mauger. K. Zaghib, C. M. Julien. *J. Power Sources*, 240 (2013) 267.
13. T. N. J. I. Edison. R. Atchudan, Y. R. Lee. *Electrochim. Acta*, 283 (2018) 1609.
14. B. Pal. S. G. Krishnan. B. L. Vijayan. M. Harilal. C.-C. Yang. F. I. Ezema. M. M. Yusoff, R. Jose. *J. Electroanal. Chem.*, 817 (2018) 217.
15. J. Jayachandiran. J. Yesuraj. M. Arivanandhan. A. Raja. S. A. Suthanthiraraj. R. Jayavel, D. Nedumaran. *J. Inorg. Organomet. Polym. Mater.*, 28 (2018) 2046.
16. E. Karaca. K. Pekmez, N. Ö. Pekmez. *Electrochim. Acta*, 273 (2018) 379.
17. Y. Lei. N. Sheng. A. Hyono. M. Ueda, T. Ohtsuka. *Prog. Org. Coat.*, 77 (2014) 774.
18. F. Fekri. M. Shahidi. M. M. Foroughi, M. Kazemipour. *J. Electrochem. Sci. Technol.*, 10 (2019) 148.
19. V. Venugopal. V. Venkatesh. R. G. Northcutt. J. Maddox, V. B. Sundaresan. *Sens. Actuators, B*, 242 (2017) 1193.
20. Z. Neisi. Z. Ansari-Asl, A. S. Dezfuli. *J. Inorg. Organomet. Polym. Mater.*, 29 (2019) 1838.
21. K. Qi. Y. Qiu. Z. Chen, X. Guo. *Corros. Sci.*, 91 (2015) 272.
22. A. El Jaouhari. M. Laabd. E. A. Bazzaoui. A. Albourine. J. I. Martins. R. Wang. G. Nagy, M. Bazzaoui. *Synth. Met.*, 209 (2015) 11.
23. H. Arabzadeh. M. Shahidi, M. M. Foroughi. *J. Electroanal. Chem.*, 807 (2017) 162.

24. M. Bazzaoui. J. I. Martins. S. C. Costa. E. A. Bazzaoui. T. C. Reis, L. Martins. *Electrochim. Acta*, 51 (2006)
25. W. Su, J. O. Iroh. *Synth. Met.*, 114 (2000) 225.
26. D. K. Ariyanayagamkumarappa, I. Zhitomirsky. *Synth. Met.*, 162 (2012) 868.
27. X. Li, I. Zhitomirsky. *Mater. Lett.*, 76 (2012) 15.
28. F. Wolfart. D. P. Dubal. M. Vidotti. R. Holze, P. Gómez-Romero. *J. Solid State Electrochem.*, 20 (2016) 901.
29. C. R. Mariappan. V. Gajraj. S. Gade. A. Kumar. S. Dsoke. S. Indris. H. Ehrenberg. G. V. Prakash, R. Jose. *J. Electroanal. Chem.*, 845 (2019) 72.
30. S. Shivakumara, N. Munichandraiah. *J. Alloys Compd.*, 787 (2019) 1044.
31. K. Karthikeyan. S. Amaresh. J. N. Son, Y. S. Lee. *J. Electrochem. Sci. Technol*, 3 (2012) 72.
32. H.-B. Zhao. L. Yuan. Z.-B. Fu. C.-Y. Wang. X. Yang. J.-Y. Zhu. J. Qu. H.-B. Chen, D. A. Schiraldi. *ACS Appl. Mater. Interfaces*, 8 (2016) 9917.
33. H. Huang. X. Zeng. W. Li. H. Wang. Q. Wang, Y. Yang. *J. Mater. Chem. A*, 2 (2014) 16516.
34. Y. Gawli. A. Banerjee. D. Dhakras. M. Deo. D. Bulani. P. Wadgaonkar. M. Shelke, S. Ogale. *Sci. Rep.*, 6 (2016) 21002.
35. W. Chen. R. B. Rakhi, H. N. Alshareef. *J. Phys. Chem. C*, 117 (2013) 15009.
36. Y. Ma. C. Hou. H. Zhang. M. Qiao. Y. Chen. H. Zhang. Q. Zhang, Z. Guo. *J. Mater. Chem. A*, 5 (2017) 14041.
37. X. Wang. J. Deng. X. Duan. D. Liu. J. Guo, P. Liu. *J. Mater. Chem. A*, 2 (2014) 12323